Am J Physiol Heart Circ Physiol 292: H3198–H3206, 2007.
First published February 16, 2007; doi:10.1152/ajpheart.01234.2006.

Live imaging of collagen remodeling during angiogenesis

Nathaniel D. Kirkpatrick,[1] Stylianos Andreou,[1] James B. Hoying,[1] and Urs Utzinger[1]

[1]*University of Arizona, Division of Biomedical Engineering, Tucson, Arizona*

Submitted 9 November 2006; accepted in final form 10 February 2007

Kirkpatrick ND, Andreou S, Hoying JB, Utzinger U. Live imaging of collagen remodeling during angiogenesis. *Am J Physiol Heart Circ Physiol* 292: H3198–H3206, 2007. First published February 16, 2007; doi:10.1152/ajpheart.01234.2006.—To better understand interstitial matrix remodeling during angiogenesis, we probed endogenous optical signatures of collagen fibrils and cells with multiphoton microscopy to noninvasively visualize, in real-time, changes to fibril organization around angiogenic sprouts and growing neovessels. From analyses of the second-harmonic generation signal from fibrillar collagen and two-photon excited fluorescence, as well as coherent transmitted light from vascular cells, we found that microvessel fragments interacting with the collagen matrix exhibited two key features: a strong association of fibrillar collagen around the parent vessel fragment during vessel construct reconstitution and a substantial collagen fibril reorganization by sprout and neovessel tips. Results indicate that angiogenic sprouts and growing neovessels actively and differentially remodel existing collagen fibrils. This imaging approach to assess local changes in matrix organization may have a broader impact on tissue biology and mechanics during angiogenesis and allow for new insights in cardiovascular, diabetes, and cancer research.

extracellular matrix; multiphoton microscopy; second harmonic generation

REMODELING OF THE extracellular matrix is an important aspect of tissue dynamics and provides critical support for vascular processes (6). Turnover of matrix and reorganization of the matrix architecture provide positional and biochemical cues to cells, as well as allow necessary movement of cells through the tissue (13, 24, 35). In angiogenesis, endothelial cells sprout from a parent vessel and advance through the tissue interstitium to establish new vessel segments (5, 26). During this process, the sprout's behavior is critically modulated by the extracellular matrix (6, 19, 33). Similarly, the sprout and, at later times, the growing neovessel affect the matrix through controlled matrix degradation and synthesis (9, 15, 20, 26). Furthermore, the process of angiogenesis is fundamentally important during development, wound healing, and tumorigenesis (2, 3, 5, 10, 16, 26). However, although endothelial cells have been shown to remodel extracellular matrix proteins in culture (21, 31), less is known concerning the effects of the angiogenic neovessels sprouting from intact vessels on matrix reorganization, in part due to the lack of real-time imaging of this interaction in an intact vessel model.

Multiphoton microscopy has increasingly shown promise in a variety of biomedical applications (4, 7, 36). Because of nonlinear excitation of endogenous chromophores in tissue, multiphoton microscopy allows for deep optical imaging of unstained and unsectioned live samples in three dimensions. In particular, second-harmonic generation (SHG) and two-photon excited fluorescence (2PEF) provide contrast between the extracellular matrix and cells (36). Fibrillar collagen, specifically type I collagen, is a major component of the extracellular matrix that can be quantitatively measured with SHG signals (34), whereas endogenous cellular 2PEF arises mainly from metabolic cofactors.

To investigate the effects of neovessel sprouting and elongation on interstitial matrix, we observed the real-time changes in collagen I fibril organization in an in vitro model of angiogenic sprouting. In this model, intact microvessel elements cultured in reconstituted type I collagen gels undergo stereotypical angiogenic sprouting whereby endothelial cells, free of mural cells, sprout from the parent vessel, and continue to grow to form a new immature neovessel (18, 27). Because the sprouting occurs in the relative absence of nonvascular cells and in a controlled temporal fashion, we were able to visualize sequential changes in collagen fibril organization using multiphoton microscopy. Cells were identified by endogenous 2PEF and by coherent transmission imaging, whereas fibrillar type I collagen was visualized by detecting SHG signals. This imaging approach enabled the nondestructive quantification and localization of alterations in collagen fibril organization during angiogenesis in intact vessels at a high resolution in three dimensions.

MATERIALS AND METHODS

Microvessel Constructs

The in vitro angiogenesis model used in our studies has been previously described elsewhere (27). Briefly, the system involves the culture of intact microvessel fragments isolated from rat adipose in a collagen gel. Epididymal fat pads from Sprague-Dawley rats were removed and digested with collagenase (2 mg/ml). Subsequent filtering of large tissue debris with a 500-μm filter and smaller debris, such as cells, with a 30-μm filter retained microvessel fragments in between this size range. Microvessel vessel fragments were then added to a solution of type I rat tail collagen (BD Biosciences, San Jose, CA) and DMEM, with everything kept on ice to keep the collagen unpolymerized. With a final concentration of 3 mg/ml collagen, 1× DMEM, and ~12,000–15,000 fragments/ml, the vessel construct solution was pH neutralized with NaOH and polymerized at 37°C within 20 min. Vessel constructs were cultured in a 48-well plate with 10% FBS-supplemented DMEM as culture medium. Angiogenesis in our system begins, predictably, at *day 3* or *4* of culture and forms a uniform vascular network by *day 14* (27). Animal procedures were performed according to University of Arizona Institutional Animal Care and Use Committee-approved protocols.

Multiphoton Microscopy

In situ imaging of microvessels. Before addition of the microvessel fragments to the collagen construct, microvessels were imaged before and after digestion from the epididymal fat pad. To image vessels in

Address for reprint requests and other correspondence: U. Utzinger, BIO5 Institute, Thomas W. Keating Bldg., 1657 E. Helen St., Tucson AZ 85724 (e-mail: utzinger@u.arizona.edu).

The costs of publication of this article were defrayed in part by the payment of page charges. The article must therefore be hereby marked "*advertisement*" in accordance with 18 U.S.C. Section 1734 solely to indicate this fact.

situ in the fat pad, the tissue was removed and smeared over a slide, and a coverslip was placed on top. For vessels after digestion, the digested microvessel solution was spread onto a slide, and a coverslip was placed on top. The samples were imaged with a 150-fs-pulsed titanium-sapphire laser (Mira 900; Coherent, Santa Clara, CA) coupled to a laser-scanning confocal microscope (LSM 510; Carl Zeiss, Jena, Germany). Incident light was focused, and emitted signals were collected with a ×40, 1.3-numerical aperture oil-immersion objective (Carl Zeiss). The laser was centered at incident wavelength (λ_{inc}) = 780 nm, and 2PEF signals were collected in the epifluorescence configuration through a custom multiphoton filter (480–580 nm; Chroma, Rockingham, VT) and onto a nondescanned photomultiplier tube (PMT) detector (based on R6357, Hamamatsu, Hamamatsu City, Japan). Similarly, the SHG signal was collected onto a second nondescan PMT detector through a custom SHG filter (380–400 nm; Chroma).

Microvessel constructs. Microvessel constructs were removed from the 48-well plate and placed in an imaging-incubation chamber consisting of temperature-controlled, oxygenated medium flowed through a custom open-imaging chamber compatible with a computer-controlled mechanical stage. Optically inert media (46 mM glucose, 4 mM glutamine, 1× PBS) was employed to reduce background autofluorescence and light absorption. A ×20, 0.95-numerical aperture long working distance objective (XLUMPFL20XW; Olympus, Tokyo, Japan) was implemented for increased imaging depth and imaging chamber compatibility. The titanium-sapphire laser was centered at λ_{inc} = 780 nm, and the typical average laser power at the back aperture of the objective was 35 mW. 2PEF and SHG signals were collected as described above with a 480- to 580-nm bandpass and a 380- to 400-nm bandpass filter, respectively. Based on our imaging setup, we collected SHG and 2PEF at depths up to 500 μm in the constructs.

Coherent transmitted near-infrared imaging. With the condenser removed, our setup allowed coherent transmission imaging where the observed contrast is based on distorted wave fronts of the excitation laser transmitting through the sample. Unfiltered transmitted light was collected onto a single PMT without any pinhole optics. The generated images illustrated cell membranes in a similar fashion as phase-contrast imaging. Because of distinct features such as morphology of sprouting vessels and their shiny appearance in coherent transmission imaging, this configuration was integral in identifying early sprouts as well as following the progression of the sprouting vessels.

Vessel Construct Perturbations

Fixed vessel imaging. Besides typical culture conditions, vessel constructs were also measured with fixed vessels. In the fixed vessel experiments, vessel fragments were isolated from the fat pad and fixed with paraformaldehyde. The fragments were then added to the collagen gel solution, and polymerized constructs were imaged on *day 0* and *day 1* of incubation.

Integrin blocking. To block integrin binding in the microvessel constructs, 10 mM cyclo-GRGDSP peptide (AnaSpec, San Jose, CA) was added to the construct before polymerization. Vessel constructs were then polymerized and imaged on *day 0* and *day 1* and compared with untreated control constructs.

Early polymerization imaging. Collagen constructs were created with the standard protocol. Instead of being polymerized in an incubator at 37°C, the prepolymerized constructs were placed in an imaging chamber and kept in an ice bath at 4°C while under the microscope. Microvessel fragments were imaged in 15-s intervals as the ice bath was brought to 37°C by a heated stage and an in-line flow heater. Before the construct polymerized, fragments were kept in the field of view by constant manual adjustment of the *x*, *y*, and *z* positions of the microscope stage.

Image Processing

For general presentation, basic image processing was applied to remove background in the SHG and 2PEF in MATLAB.

For all quantitative measurements, unprocessed images were analyzed with a custom-designed MATLAB program and routines made available in the public domain. The program allows users to select areas in the microscopy images to determine regions of interest (ROI) for image statistics and collagen concentration profiles based on SHG intensity, as well as on sprouting vessel and collagen fibril orientations. Reference areas were selected for comparison to ROIs. For collagen concentration estimates around the parent vessels, a polygon ROI was drawn manually around the entire border of the vessel in an image plane that best represented the center of the vessel, and the SHG intensity was calculated in this region. This ROI encompassed only the region immediately adjacent to the vessel. To correct for intensity differences due to interexperimental variations (i.e., laser power, vessel depth, collagen gel differences), a reference region with collagen fibrils in the same field of view, but away from vessels or any other cells, was also defined, and the SHG intensity was calculated. SHG intensity is nonlinearly proportional to the collagen content, such that under ideal conditions the intensity scales quadratically with the proportion of fibrils aligned to the incident polarization (8, 28). To estimate spatial collagen concentration, SHG intensity profiles across the parent vessels and neovessels were calculated by drawing a 5-μm-wide line perpendicular to the vessel and computing the average SHG intensity with a resolution of ~0.5 μm along the line. These profiles were normalized by their maximum intensity to compare between multiple vessels. For neovessel profiles in the middle and base regions, the profile was computed in an image slice where visible SHG increases occurred along the endothelial cells.

In the case of vessels sprouting into the collagen and remodeling the matrix, collagen fibril orientation was calculated based on a modified ridge detection algorithm that determines ridge direction from local image gradients and subsequent continuous vector field generation (17, 22). Briefly, SHG images were first normalized to have a mean of zero and standard deviation of 1. Next, the image gradients were calculated in the *x* and *y* directions by applying a Gaussian-based Sobel filter to the image in the *x* and *y* directions. The fibril orientation at each point was determined by finding the principal axis of variation based on the covariance of these image gradients. Local orientations were calculated by smoothing the covariance data with another Gaussian filter that found the average local orientation for a specified region size around the pixel of interest. Finally, the principal axis of direction for each local region within the image was determined analytically by applying the smoothed covariance data for the image gradients to the solutions provided in Hong et al. (17). In addition to calculating local fibril orientations, we also determined whether fibrils existed within a local region based on a reliability measure that compared the area moment of the inertia about the calculated principal direction to the area moment of inertia about the perpendicular direction. We only used orientation data where there was useful orientation information; in other words, the reliability indicated minimal inertia in the principal axis direction compared with the perpendicular direction. To compare fibril direction with direction of sprouting vessels, we manually determined the sprouting vessel direction from the transmission image. For each sprout analyzed, an ROI was drawn manually around the sprout tip, and a reference region from the same field of view, approximately the same area as the ROI, was manually selected in a region away from the sprout.

Statistics

To compare the orientation of fibrils in the ROI around the sprouting tips with the orientation of a reference region, two measures were computed in MATLAB. First, the absolute angle between the mean fibril orientation of the ROI or reference region and the vessel direction was calculated (mean fibril direction in ROI − sprout direction, denoted as fibril deviation). Next, the second moment of the angular distribution of fibril orientation was calculated to estimate the variation in either the ROI or reference region (denoted as fibril

variation). The second moment was used instead of the standard deviation because the angular distributions were not all normally distributed and because the second moment provided a more robust measure of the variation in distributions that were not normal. These two variables, the fibril deviation and variation, along with the culture day (i.e., *day 3*, *day 4*, etc.), were used for further analyses between the ROI and reference regions of sprouts and neovessels on different culture days using the JMP software platform (SAS Institute, Cary, NC). Data were log-log transformed to meet the criteria of equal variability between the test groups. Data were determined to be normally distributed with the normal quantile plot function. Statistical differences between the ROI and reference regions were calculated based on a Wilk's lambda test.

RESULTS

Collagen Association With Parent Microvessels

In the angiogenic sprouting model, microvessel fragments freshly isolated from adipose were suspended in pH-neutral-

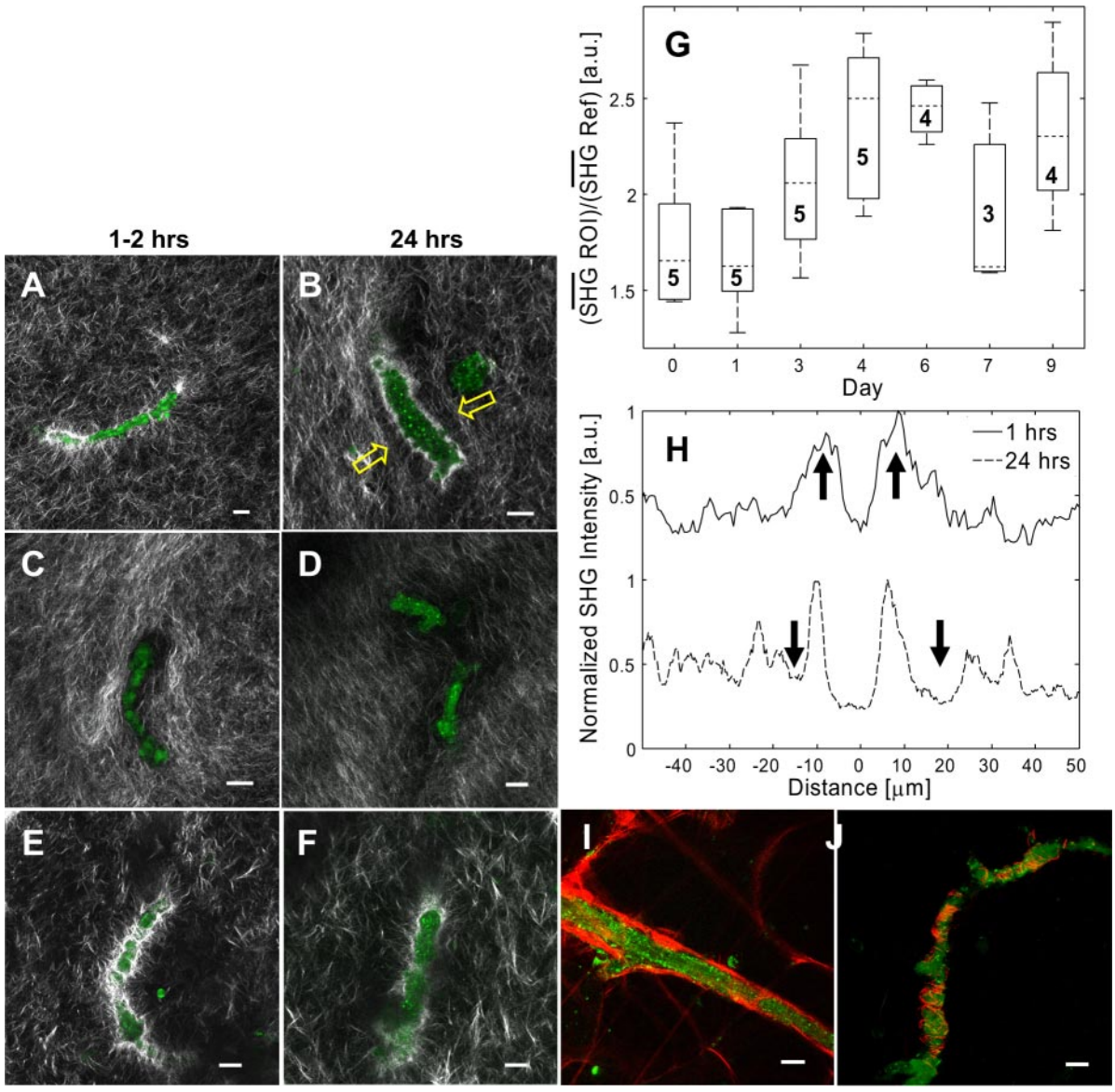

Fig. 1. Microvessel associations with a collagen matrix. Imaging parameters: λ_{inc} = 780 nm, λ_{SHG} = 380–400 nm, λ_{2PEF} = 480–580 nm, where λ is wavelength, inc is incident, SHG is second-harmonic generation, and 2PEF is 2-photon excited fluorescence. Scale bar = 20 μm. *A*: after polymerization of the gel (1–2 h), vessel fragments interacted strongly with the collagen matrix with bright SHG (grayscale) observed at the vessel wall (2PEF, green). *B*: after 24 h of culture, collagen-depleted regions form around vessel fragments (arrows). *C* and *D*: fragments fixed with paraformaldehyde show little interaction with collagen at early (1–2 h; *C*) and later (24 h; *D*) time points. *E* and *F*: 10 mM cyclic RGD peptide failed to page collagen condensation at 1–2 h (*E*) and after 24 h (*F*). *G*: quantitative analysis of mean SHG (SHG) intensity ratios from regions of interest (ROIs) at the vessel wall to reference regions indicate an increase in collagen concentration around the vessel with culture time, but remaining relatively constant after *day 4* (box-and-whisker diagram). au, Arbitrary unit. *H*: SHG profiles (intensity normalized and centered at the vessel middle) from vessel fragments observed in *A* and *B* highlight the early condensed collagen and subsequent formation of a depleted region (arrows). *I*: microvessel/collagen association in its native environment reveals a substantial amount of collagen around the vessel wall (native SHG pseudocolored red). *J*: after vessel extraction, residual collagen surrounds a fragment in a helical fashion (3-dimensional projection). This particular example had higher residual collagen SHG signal than typically observed in other isolated microvessel fragments, suggesting that this fragment would be near the maximal amount of residual collagen that we could expect.

ized, cold collagen I and then placed at 37°C to promote collagen polymerization. To understand how the polymerizing collagen interacted with the parent microvessel fragments, we imaged the early polymerization events focusing on the interface between microvessel fragment and collagen. We observed a hyperintense SHG signal consistent with a concentrated amount of fibrillar collagen associated with the parent vessels immediately on reconstitution within the forming collagen gel (Fig. 1*A* and *supplementary movie 1*). (The online version of this article contains supplemental data.) Within 1 day of culture, the pronounced SHG signal remained around the vessel and localized to the perivascular cells. Also, a region of depleted signal appeared around the vessel fragment (Fig. 1*B*, arrows). To determine whether this collagen condensation process was active or passive, we fixed freshly isolated microvessel fragments with paraformaldehyde before collagen reconstitution. Fixed microvessels showed minimal interaction with the collagen fibrils after polymerization (Fig. 1*C*) or after 1 day (Fig. 1*D*). The relative collagen content, as estimated by the SHG intensity ratio, an index of collagen content (see MATERIALS AND METHODS) of the region immediately surrounding the microvessels, was much less in the prefixed microvessels than in the live vessels (0.676 ± 0.12, $n = 6$, for fixed vessels; 1.71 ± 0.31, $n = 10$, for live vessels; both for *day 0* and *day 1* vessels). These data suggested that the collagen association with the parent vessel wall requires biological activity. However, the presence of an excess (10 mM) of the cyclo-GRGDSP peptide (RGD), a potent inhibitor of integrin-collagen binding (12), during polymerization did not disrupt the association of collagen to the parent microvessel fragments (Fig. 1, *E* and *F*) because the SHG intensity ratios were similar between RGD-treated and untreated microvessel constructs (1.97 ± 0.41, $n = 5$, for RGD treated; 1.71 ± 0.31, $n = 10$, for untreated; both for *day 0* and *day 1* vessels). Concentrated collagen at the vessel wall was present as early as *day 0*, increased until *day 4*, and remained relatively constant for the rest of the culture period (Fig. 1). Representative profiles of SHG intensity ratios across the microvessel width from Fig. 1*A* and Fig. 1*B*, respectively, revealed the formation of zones depleted in collagen neighboring the areas of collagen condensation at the vessel walls by 24 h after polymerization (Fig. 1*H*, arrows). However, these regions of depleted collagen were not consistently observed.

We next examined the collagen organization around microvessels within the intact adipose tissue to see whether the collagen organization observed in the cultured microvessel-collagen constructs resembled that present in the native tissue. Similar to the collagen condensation observed in the constructs, microvessels in the adipose tissue also exhibited a pronounced layer of collagen (Fig. 1*I*). We could rule out that the fibrillar collagen observed in the cultures was due to collagen remaining on the fragments after isolation because three-dimensional projections of the SHG signal from fibrillar collagen surrounding the freshly isolated microvessel revealed only residual strands of collagen (Fig. 1*J,* representing an example with high residual collagen content).

We further investigated the interaction of collagen fibrils with microvessel fragments during construct polymerization with time-lapse microscopy. We followed microvessels suspended in cold collagen solution followed by the induction of collagen polymerization by increasing the temperature (Fig. 2 and *supplementary movie 1*). The microvessel fragment in the prepolymerized collagen solution exhibited minimal SHG-related residual collagen (Fig. 2, *time 0*). However, as the collagen began to polymerize, initial fibrils formed (i.e., there was an increase in SHG signal intensity) in direct association with the microvessels. Interestingly, this polymerization associated with the vessels occurred before a clear presence of fibrils in the gel space near the vessels. By the time the collagen construct was completely polymerized, a condensed collagen layer had formed around the microvessel fragment (Fig. 2). These results indicate that collagen deposition is initially preferred on the intact microvessel surface with further condensation continuing after polymerization (Fig. 1*G*).

Matrix Remodeling at Angiogenic Sprout Tips

We next examined collagen fibril architecture around angiogenic sprout and growing neovessel tips in the constructs. During early sprouting at *days 3* and *4*, endothelial cells extended out from the parent vessel forming the initial leading tip of the sprout (Fig. 3, *A* and *C*, arrow) while aligning collagen fibrils in a fanlike pattern with fibrils radiating out from the sprout tip into the matrix in the direction of the sprout (Fig. 3, *B* and *D*). Collagen fibril realignment toward the tip of these early sprouts extended well beyond the length of the early sprout, suggesting high fibril mobility along with dynamic fibril interactions. This fanlike distribution of fibrils was apparent in three dimensions as the fibrils organized above and below the microvessel sprouts (Fig. 3*I*). Often, a single parent

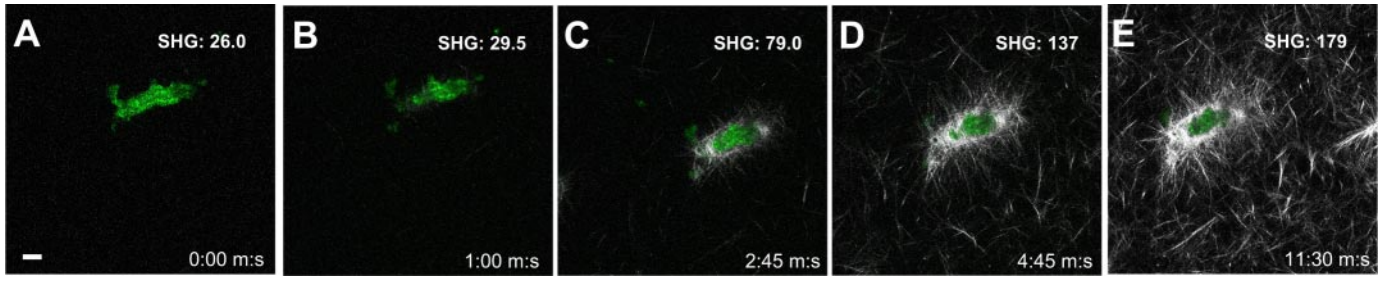

Fig. 2. Immediate collagen condensation during polymerization at the microvessel wall. Imaging parameters: $\lambda_{inc} = 780$ nm, $\lambda_{SHG} = 380–400$ nm, $\lambda_{2PEF} = 480–580$ nm. Scale bar = 20 μm; time stamp in minutes:seconds. SHG intensity from region adjacent to microvessel fragment is in arbitrary units. *A*: microvessel fragment (2PEF, green) in prepolymerized collagen reveals minimal SHG signal (grayscale). *B*: after ~1 min, the collagen construct begins to polymerize, with the first fibrils appearing around the microvessel fragment. *C*: polymerization proceeds rapidly with continued condensation at microvessel, as shown with increased SHG intensity. *D*: fibrils form in the region away from the microvessel, but condensation continues to increase at the microvessel. *E*: by 11 min, 30 s, the construct is completely polymerized, with maximal collagen condensation surrounding the microvessel.

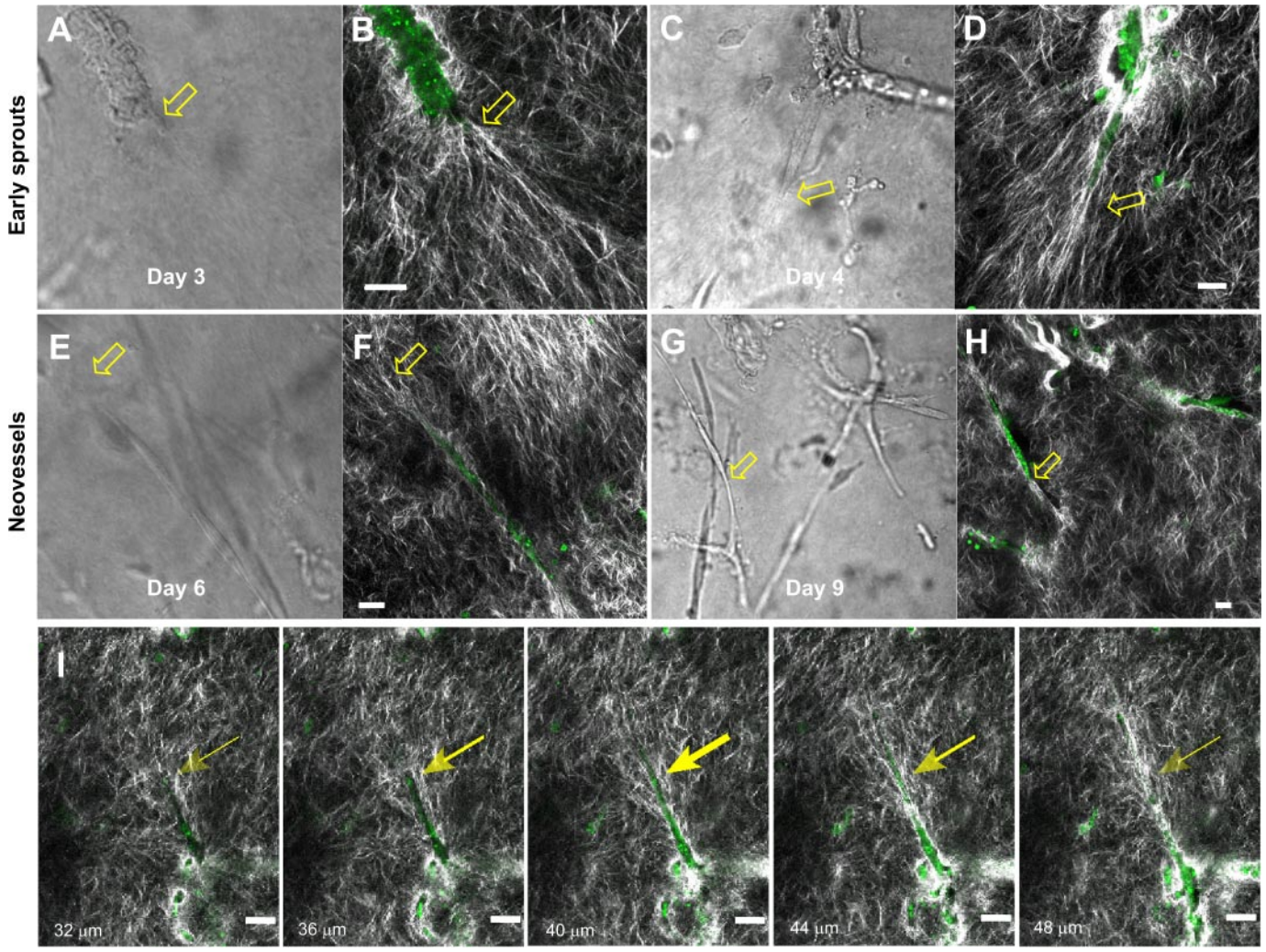

Fig. 3. By *day 3* and *day 4* of culture, microvessel fragments form early sprouts, modifying the collagen matrix. Imaging parameters: λ_{inc} = 780 nm, λ_{SHG} = 380–400 nm, λ_{2PEF} = 480–580 nm, transmission (λ_{trans}) = unfiltered. Scale bar = 20 μm. *A*: in transmission, an endothelial cell extension of an early sprout appears at the end of a parent fragment (arrow). *B*: the protruding cell body exhibits 2PEF (green) and rearranges collagen fibrils (SHG, grayscale) well beyond the parent vessel. *C*: a pointed, smooth sprout further extends from the bumpy-appearing parent vessel, modifying the collagen fibrils into a fan pattern (*D*). *E*: as sprouts continue to extend and proliferate, long enough to cover the field of view, we consider them neovessels. *F*: fibrils appear attached (arrow) at the end of a neovessel but not to the extent observed during early sprouting. *G*: multiple neovessels are observed in a single field of view on *day 9*. *H*: one of the neovessels forms extended adhesions with collagen fibrils along its body (arrow). *I*: series of image slices illustrate the collagen fibril rearrangement around an early sprout in the axial dimension (slice depth indicated in μm). The emboldened arrow signifies the center of the sprout.

fragment contained multiple sprouts, each of which reorganized collagen fibrils to some degree (*supplementary movie 2*) (The online version of this article contains supplemental data.)

By *day 6*, microvessel sprouts continued to grow and extend away from the parent vessel forming neovessels (Fig. 3*E*). In these neovessels, the tip continued to reorganize the preceding collagen fibrils but less noticeably compared with *days 3* and *4* early sprouts (Fig. 3*F*). By *day 9* of culture, the neovessel growth was substantial with multiple neovessels visible in a single field of view (Fig. 3*G*) and collagen aligned in areas along the neovessels (Fig. 3*H*, arrow). In the neovessels the distribution of collagen along the vessel varied depending on the location in relation to the parent vessel. At the neovessel tip (region furthest from the parent vessel) minimal collagen condensation was apparent, whereas the middle region exhibited an increase in collagen and the base (region adjacent to parent vessel) exhibited an even greater association with collagen (Fig. 4).

Quantitative Assessment of Collagen Fibril Rearrangement

We further assessed collagen fibril orientation adjacent to sprout and neovessel tips via a custom program incorporating a modified ridge-based texture algorithm that determines ridge (collagen fibril) direction from local gradient fields and subsequent continuous vector field generation (17). An overlay of the fibril vector field with the multiphoton image revealed preferentially directed regions of fibrils surrounding the microvessel sprout (Fig. 5*A*) and distributing uniformly along the general axis of the sprout extension (Fig. 5*B*). More specifically, calculation of the average fibril direction normalized to the direction of the microvessel sprout (fibril deviation) and the distribution of fibril angles (fibril variation) in an ROI at the sprout suggested that fibril angles at the end of sprouts were dramatically rearranged in the direction of the sprout (Fig. 5*C*), significantly differing from fibril distributions in regions away from sprouts (P = 0.0024, Wilk's lambda, n = 16). At the tip

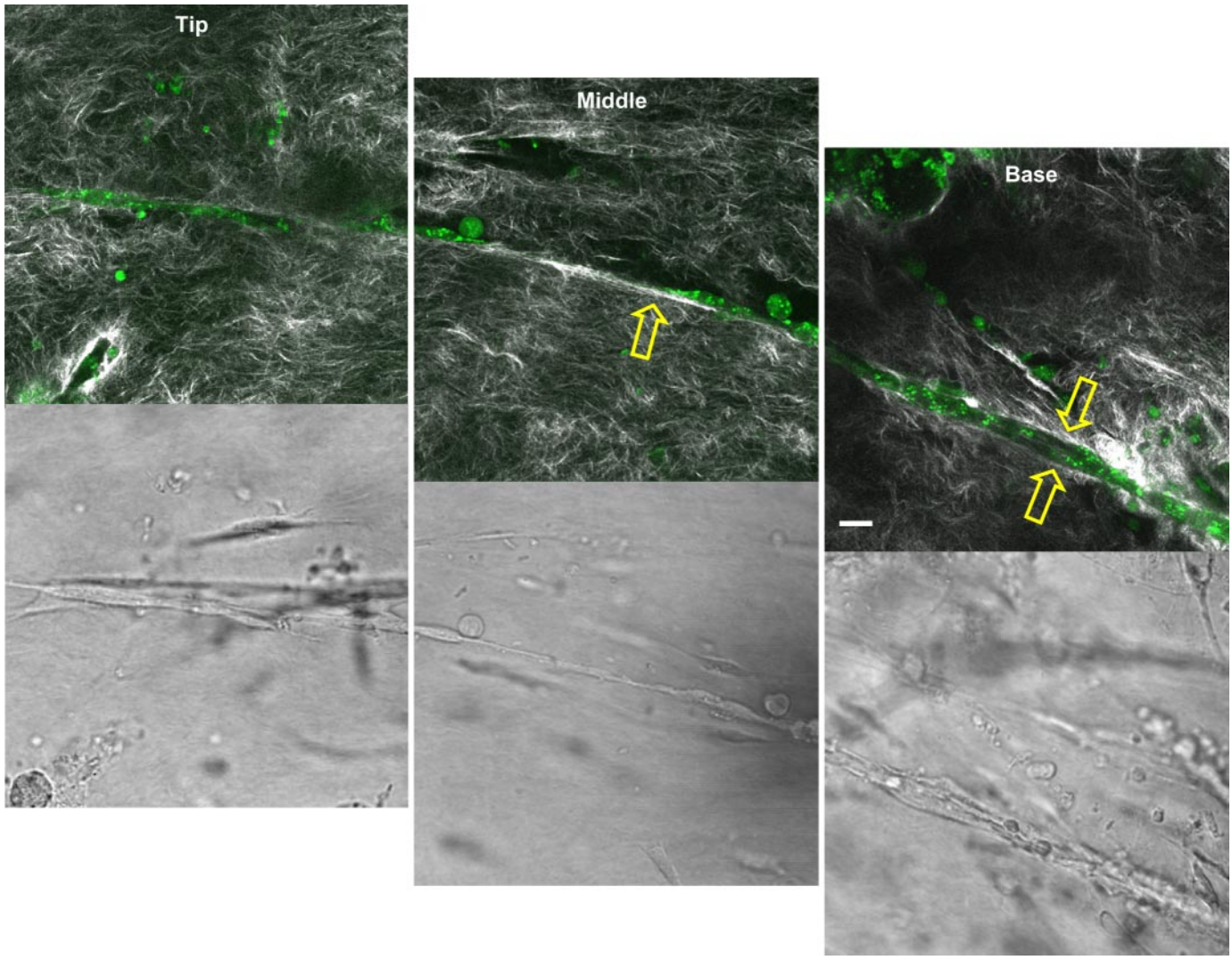

Fig. 4. Fibrillar collagen distribution varied in neovessels. Imaging parameters: λ_{inc} = 780 nm, λ_{SHG} = 380–400 nm, λ_{2PEF} = 480–580 nm, λ_{trans} = unfiltered. Scale bar = 20 μm. We divided neovessels into the three regions: the tip, middle, and base. A long neovessel on *day 9* shows little association with the collagen (SHG, grayscale) at the tip but exhibits a strong SHG signal along one side of the neovessel in the middle region (arrow), whereas at the base, where the neovessel leaves the parent vessel, collagen SHG signal localizes along both sides of the sprout (double arrows).

of growing neovessels (i.e., *days 6–9*), fibrils were still orientated toward the axis of neovessel elongation (Fig. 5*D*). However, there was less uniformity in fibril directions, particularly with neovessels from *day 7* and *day 9* cultures (Fig. 5*D*). Despite the less directed fibril orientation at the sprout tips at later culture days, the fibril orientation around the neovessel tips remained significantly different compared with regions away from microvessel structures ($P = 0.013$, Wilk's lambda, $n = 24$). However, the oriented fibrils at the neovessel tips did not extend as far away from the tips as observed in the early sprouts.

We next analyzed the variation in collagen alignment illustrated in Fig. 4 with SHG intensity profiles cross-sectional to neovessels to assess the distribution of collagen condensation at the middle and base regions of the growing neovessels. In general, fibrillar collagen (bright SHG signals) was condensed along the growing neovessel in the middle and base regions (Fig. 4). However, collagen fibrils uniformly surrounded the neovessel at the base of the growing neovessel (i.e., near the parent vessel) (Fig. 5*E*). On the other hand, in the middle regions of neovessels, much narrower in dimension than the base regions, collagen consistently condensed along a single side of the sprout (Figs. 5, *F* and *G*), suggesting a unilateral process in this region.

DISCUSSION

Previous in vitro models of angiogenesis have provided valuable insight into the importance of the extracellular matrix on endothelial cell migration and morphogenesis as well as endothelial cell-induced extracellular matrix remodeling (1, 21, 31–33). For example, Korff and Augustin (21) examined cell elongation from endothelial spheroids and determined that collagen fibril alignment was due to the endothelial cells. However, these models have been limited to observation of cultured endothelial cells and do not capture angiogenesis in an intact vessel where an endothelial cell must first break through the basement membrane and then negotiate a new environment

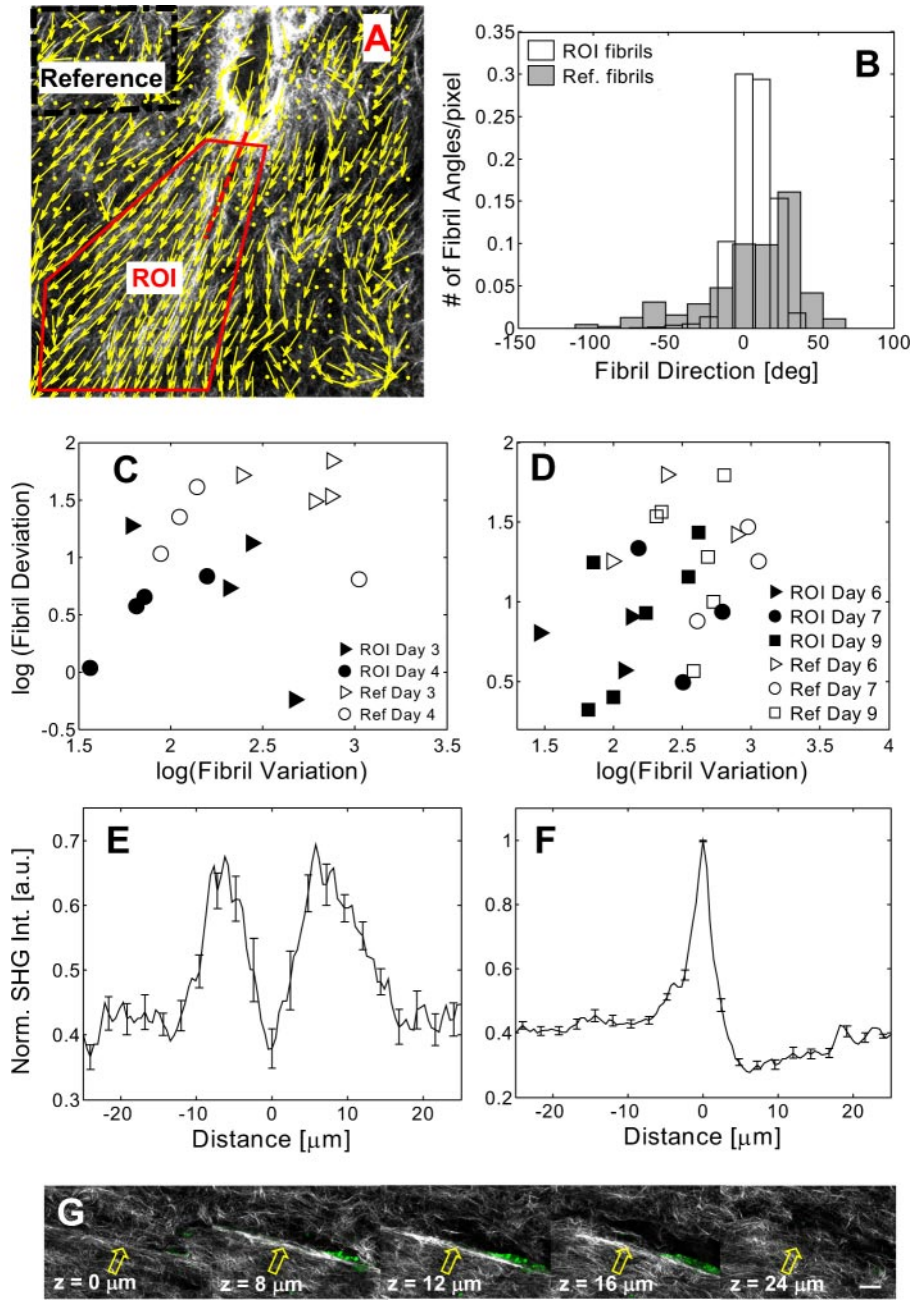

Fig. 5. Quantification of the collagen fibril orientation near the early sprouting vessels suggests collagen fibrils orient in a fanlike pattern centered about the direction of the sprout, whereas neovessels exhibit varied associations with collagen. *A*: we determined fibril orientation (yellow arrows) with a modified ridge detection algorithm, as illustrated with the sprout from Fig. 3*D*. For display purposes only, one-half of the calculated orientation arrows are shown. Areas in the image not reaching a reliability threshold for a detected fibril were not used (yellow dots). We selected a sprout ROI (red line), a reference region (dashed black line), and a sprouting vessel direction (dashed red line). *B*: histogram of the calculated fibril angles centered about the sprouting vessel direction indicates the ROI fibrils center tightly about the sprout direction compared with the reference (Ref) region. deg, Degree. *C*: with ordinate indicating deviation from sprouting direction and abscissa indicating spread of fibril orientation, significant collagen fibril modification at the early sprout tips is shown ($P = 0.0024$, Wilk's lambda, $n = 16$). Data were log-log transformed to ensure equal variation between groups. *D*: neovessel tips that have extended away from the parent vessel exhibit less dramatic but still significant fibril modifications ($P = 0.013$, Wilk's lambda, $n = 24$). *E*: at the base of neovessels near the parent vessel, profiles [intensity (int) normalized (norm) and centered at sprout center] indicate a uniform collagen layer surrounding the neovessel (SE bars, $n = 7$). *F*: profiles (intensity normalized and centered at neovessel side) for the middle regions suggest a unilateral distribution of collagen around the sprout (SE bars, $n = 9$). *G*: by *z*-stepping through the middle region of a neovessel, we found increased collagen condensation primarily along one side of the neovessel. Scale bar = 20 μm.

dominated by type I collagen fibrils. Here, we extend research of matrix remodeling by endothelial cells by introducing the ability to directly visualize microvessel-matrix interactions in a dynamic and quantitative manner in live intact microvessels.

Before assessing collagen remodeling during angiogenic events, we found initial interactions between parent vessels and the collagen fibrils resulting in a condensed layer of collagen around the parent vessel on polymerization. Although the collagen condensation required live vessels, it was not blocked by cyclic RGD and also occurred immediately at the onset of collagen polymerization. Several factors could account for the immediate collagen attachment and condensation around the vessel fragments. The vessels, particularly the perivascular cells, may provide polymerization or nucleation sites for the fibrils to assemble independent of integrin binding. The basis for this is not known, but it is possible that collagen-binding surfaces and matrix molecules could act as a polymerization nidus (23). In this regard, residual native collagen remaining on the vessel fragments after collagenase digestion may add polymerization sites near the vessel. However, because there was only a minimal amount of residual collagen, this seems less likely. Other extracellular proteins such as fibronectin (30) in the intact basement membranes of the parent vessels may also provide polymerization sites. Because collagen condensation coincided with collagen polymerization, it may be that in the intact tissue, collagen that is newly synthesized and secreted by vascular cells may rapidly polymerize and associate with the vessel wall. This would ensure an immediate, new extracellular matrix environment would be in place to accommodate any necessary changes in vessel phenotype.

Beyond the relationship between the parent vessels and the collagen matrix, we found key interactions between sprouting microvessels and collagen fibrils that may provide indications of crucial matrix related events during angiogenesis. Depending on the location along the vessel structure, we observed differential fibril alignment patterns. At the tip of nascent sprouts or advancing neovessels, collagen fibrils were aligned toward the vessel as if being pulled to the tip most likely through integrin binding (21, 25). Although it is not yet clear what role the collagen fibril reorganization plays during neovessel sprouting, we hypothesize that the remodeling by the early sprouts and neovessel tips is a normal process in the initial sprouting event. The tip endothelial cell extends filopodia into the surrounding matrix (14), which is thought to provide directional anchors for the subsequent forward migration of the sprout (29). As the cell moves forward, tension would be placed on the fibrils attached to these filopodia and, if free to move, reorient toward the sprout tip. Additionally, the realignment of the fibrils may also create a pathway through the matrix, facilitating directed sprout advancement because migration of cells along rigid constituents is preferred (11, 24). We predict that the observed fibril rearrangement occurs in vivo during angiogenesis but perhaps not as dramatically because fibrillar collagen in the in vivo interstitium will likely be enzymatically cross-linked and bound to an additional meshwork of matrix molecules.

In addition to fibril realignment at sprout and neovessel tips, we observed significant association of fibrillar collagen along neovessel structures. Given the presence of a similar fibrillar layer in the mature adipose microvessels (Fig. 1*I*), we hypothesize that this association during angiogenesis is a precursor of postangiogenesis maturation. We propose that the layering of fibrillar collagen along the midregions of the growing neovessel, where the vessel is narrow and had only recently grown into the matrix, comes from the existing fibrils reoriented by the neovessel tip that have remained associated with the neovessel as it advanced. This passive association between existing fibrils and growing neovessels might result in a nonuniform distribution of collagen, consistent with our observations. On the other hand, the collagen layer associated with the neovessel base, which is an older and likely more mature structure, is perhaps due to new collagen deposition creating a more uniformly distributed collagen layer. Our observation that a biologically active vessel surface acts as a nidus for type I collagen polymerization further suggests that, if new collagen is synthesized in proximity to microvessel, it will condense preferentially and uniformly around the vessels. Prolonged time-lapse videomicroscopy of the growing neovessel should prove useful in addressing this issue.

Together, these results suggest a dynamic modulation of extracellular fibrillar collagen by intact angiogenic neovessels captured by multiphoton microscopy of endogenous signals that reflects different aspects of neovessel formation and progression from remodeling of collagen fibrils during early sprouting events to increased collagen condensation in developing neovessels. Applying this model of angiogenesis combined with vital multiphoton imaging creates an avenue for further insights into matrix dynamics and underlying molecular mechanisms. Given the significant role that the matrix plays in modulating angiogenic behavior, these changes in collagen organization likely contribute to neovessel behavior. Whether these local changes in matrix organization have a broader impact on tissue biology and mechanics during angiogenesis remains to be determined.

ACKNOWLEDGMENTS

We thank Harish Rekapally and Shaleen Botting for assistance with the vessel constructs. We also thank Dr. Arthur Gmitro for discussions concerning coherent transmission microscopy and Livia Zarnescu for data analysis assistance.

GRANTS

This work was supported by National Institutes of Health Grants HL-077683, HL-67067, HL-007955, and CA-098341.

REFERENCES

1. **Arthur WT, Vernon RB, Sage EH, Reed MJ.** Growth factors reverse the impaired sprouting of microvessels from aged mice. *Microvasc Res* 55: 260–270, 1998.
2. **Battegay EJ.** Angiogenesis: mechanistic insights, neovascular diseases, and therapeutic prospects. *J Mol Med* 73: 333–346, 1995.
3. **Blavier L, Henriet P, Imren S, Declerck YA.** Tissue inhibitors of matrix metalloproteinases in cancer. *Ann NY Acad Sci* 878: 108–119, 1999.
4. **Brown E, McKee T, diTomaso E, Pluen A, Seed B, Boucher Y, Jain RK.** Dynamic imaging of collagen and its modulation in tumors in vivo using second-harmonic generation. *Nat Med* 9: 796–800, 2003.
5. **Carmeliet P.** Angiogenesis in life, disease and medicine. *Nature* 438: 932–936, 2005.
6. **Davis GE, Senger DR.** Endothelial extracellular matrix: biosynthesis, remodeling, and functions during vascular morphogenesis and neovessel stabilization. *Circ Res* 97: 1093–1107, 2005.
7. **Denk W, Strickler JH, Webb WW.** Two-photon laser scanning fluorescence microscopy. *Science* 248: 73–76, 1990.
8. **Donnelly E, Williams RM, Downs SA, Dickinson ME, Baker SP, van der Meulen MCH.** Quasistatic and dynamic nanomechanical properties of cancellous bone tissue relate to collagen content and organization. *J Mater Res* 21: 2106–2117, 2006.
9. **Fisher C, Gilbertson-Beadling S, Powers EA, Petzold G, Poorman R, Mitchell MA.** Interstitial collagenase is required for angiogenesis in vitro. *Dev Biol* 162: 499–510, 1994.
10. **Folkman J.** Angiogenesis in cancer, vascular, rheumatoid and other disease. *Nat Med* 1: 27–31, 1995.
11. **Friedl P, Brocker EB.** The biology of cell locomotion within three-dimensional extracellular matrix. *Cell Mol Life Sci* 57: 41–64, 2000.
12. **Garnotel R, Monboisse JC, Randoux A, Haye B, Borel JP.** The binding of type I collagen to lymphocyte function-associated antigen (LFA) 1 integrin triggers the respiratory burst of human polymorphonuclear neutrophils. Role of calcium signaling and tyrosine phosphorylation of LFA 1. *J Biol Chem* 270: 27495–27503, 1995.
13. **Geiger B, Bershadsky A, Pankov R, Yamada KM.** Transmembrane crosstalk between the extracellular matrix—cytoskeleton crosstalk. *Nat Rev Molec Cell Biol* 2: 793–805, 2001.
14. **Gerhardt H, Golding M, Fruttiger M, Ruhrberg C, Lundkvist A, Abramsson A, Jeltsch M, Mitchell C, Alitalo K, Shima D, Betsholtz C.** VEGF guides angiogenic sprouting utilizing endothelial tip cell filopodia. *J Cell Biol* 161: 1163–1177, 2003.
15. **Haas TL, Davis SJ, Madri JA.** Three-dimensional type I collagen lattices induce coordinate expression of matrix metalloproteinases MT1-MMP and MMP-2 in microvascular endothelial cells. *J Biol Chem* 273: 3604–3610, 1998.
16. **Holmgren L, Glaser A, Pfeifer-Ohlsson S, Ohlsson R.** Angiogenesis during human extraembryonic development involves the spatiotemporal control of PDGF ligand and receptor gene expression. *Development* 113: 749–754, 1991.
17. **Hong L, Wan YF, Jain A.** Fingerprint image enhancement: algorithm and performance evaluation. *IEEE Trans Pattern Anal Machine Intell* 20: 777–789, 1998.
18. **Hoying JB, Boswell CA, Williams SK.** Angiogenic potential of microvessel fragments established in three-dimensional collagen gels. *In Vitro Cell Dev Biol Anim* 32: 402–419, 1996.
19. **Ingber DE.** Mechanical signaling and the cellular response to extracellular matrix in angiogenesis and cardiovascular physiology. *Circ Res* 91: 877–887, 2002.

20. **Jain A, Nanchahal J, Troeberg L, Green P, Brennan F.** Production of cytokines, vascular endothelial growth factor, matrix metalloproteinases, and tissue inhibitor of metalloproteinases 1 by tenosynovium demonstrates its potential for tendon destruction in rheumatoid arthritis. *Arthritis Rheum* 44: 1754–1760, 2001.
21. **Korff T, Augustin HG.** Tensional forces in fibrillar extracellular matrices control directional capillary sprouting. *J Cell Sci* 112: 3249–3258, 1999.
22. **Kovesi PD.** *MATLAB and Octave Functions for Computer Vision and Image Processing [Matlab Code]*. Crawley, Australia: School of Computer Science & Software Engineering, The Univ. of Western Australia, 2005. http://www.csse.uwa.edu.au/~pk/research/matlabfns/.
23. **Lee P, Lin R, Moon J, Lee LP.** Microfluidic alignment of collagen fibers for in vitro cell culture. *Biomed Microdevices* 8: 35–41, 2006.
24. **Lo CM, Wang HB, Dembo M, Wang YL.** Cell movement is guided by the rigidity of the substrate. *Biophys J* 79: 144–152, 2000.
25. **Nisato RE, Tille JC, Jonczyk A, Goodman SL, Pepper MS.** αvβ3 and αvβ5 integrin antagonists inhibit angiogenesis in vitro. *Angiogenesis* 6: 105–119, 2003.
26. **Risau W.** Mechanisms of angiogenesis. *Nature* 386: 671–674, 1997.
27. **Shepherd BR, Chen HY, Smith CM, Gruionu G, Williams SK, Hoying JB.** Rapid perfusion and network remodeling in a microvascular construct after implantation. *Arterioscler Thromb Vasc Biol* 24: 898–904, 2004.
28. **Stoller P, Reiser KM, Celliers PM, Rubenchik AM.** Polarization-modulated second harmonic generation in collagen. *Biophys J* 82: 3330–3342, 2002.
29. **Sun S, Wheeler MF, Obeyesekere M, Patrick CW Jr.** A deterministic model of growth factor-induced angiogenesis. *Bull Math Biol* 67: 313–337, 2005.
30. **Velling T, Risteli J, Wennerberg K, Mosher DF, Johansson S.** Polymerization of type I and III collagens is dependent on fibronectin and enhanced by integrins α11β1 and α2β1. *J Biol Chem* 277: 37377–37381, 2002.
31. **Vernon RB, Angello JC, Iruela-Arispe ML, Lane TF, Sage EH.** Reorganization of basement membrane matrices by cellular traction promotes the formation of cellular networks in vitro. *Lab Invest* 66: 536–547, 1992.
32. **Vernon RB, Sage EH.** A novel, quantitative model for study of endothelial cell migration and sprout formation within three-dimensional collagen matrices. *Microvasc Res* 57: 118–133, 1999.
33. **Whelan MC, Senger DR.** Collagen I initiates endothelial cell morphogenesis by inducing actin polymerization through suppression of cyclic AMP and protein kinase A. *J Biol Chem* 278: 327–334, 2003.
34. **Williams RM, Zipfel WR, Webb WW.** Interpreting second-harmonic generation images of collagen I fibrils. *Biophys J* 88: 1377–1386, 2005.
35. **Woessner JF Jr.** Matrix metalloproteinases and their inhibitors in connective tissue remodeling. *FASEB J* 5: 2145–2154, 1991.
36. **Zipfel WR, Williams RM, Webb WW.** Nonlinear magic: multiphoton microscopy in the biosciences. *Nat Biotechnol* 21: 1369–1377, 2003.